



RESEARCH ARTICLE

Design of the five-bar linkage with singularity-free workspace

Tivadar Demjen¹, Erwin-Christian Lovasz¹ , Marco Ceccarelli² , Carmen Sticlaru¹, Antonio-Marius-Flavius Lupuți¹, Alexandru Oarcea¹ and Dan-Cristian Silaghi-Perju¹

¹Department of Mechatronics, Politehnica University of Timișoara, Timișoara, Romania and ²LARM² Laboratory of Robot Mechatronics, University of Rome Tor Vergata, Roma, Italy

Corresponding author: Erwin-Christian Lovasz; Email: erwin.lovasz@upt.ro

Received: 29 January 2023; **Revised:** 6 June 2023; **Accepted:** 5 July 2023; **First published online:** 11 August 2023

Keywords: five-bar linkage; analysis; synthesis; performance indices; mechanism prototype

Abstract

This paper shows the kinematic analysis and the synthesis of the five-bar linkage with symmetrical structure and singularity-free dexterous workspace. The type synthesis of the five-bar linkage shows that the number of symmetrical structures of five-bar linkage is limited to eight structures. This study deals with the forward and inverse kinematic analysis and synthesis of the five-bar structure 5-RRRRR. The synthesis equations allow the analytical computation of the link lengths of a symmetrical five-bar linkage using only revolute joints to avoid the singularities in an imposed dexterous workspace. A numerical example of the symmetrical five-bar linkage is analyzed and synthesized theoretically and characterized by computing the performance indices. The tests on an experimental model of the five-bar linkage 5-RRRRR confirm the singularity-free dexterous workspace.

1. Introduction

Five-bar linkages are simple mechanisms with 2 degrees of freedom (DoF), which allow the generation of planar paths for the characteristic point by correlation and control between the motions of the two servomotors. Although the history of the five-bar linkages is complex, with a multitude of applications and fields of implementation, in the late years we could see that there are still unexplored and undocumented uses that popped-up for niche applications. Some of these applications are prosthetics, industrial machines, haptic devices, five-bar manipulators, 3D printers, and others. Tempea et al. proposed a mechanism with five bars in general and a degenerative form as the acting solution of a SCARA robot [1]. Tsetserukou et al. developed a device where the mechanism is used in an assembly for virtual reality (further referred as VR) experience enhancement and as feedback from the VR world to the real one. In this application, the authors used an inverted five-bar linkage with a set of electric motors to build their device [2]. Marzouk et al. used a double crank five-bar linkage for a polycentric knee joint with spring swing phase control [3]. Other applications in fields such as agriculture research also made use of the five-bar linkage in the past years. As an example of this, Sun et al. [4] presented a possible solution for an automatic transplanter device. Sengqi Jian in his master's degree thesis [5] developed a five-bar robot used for pressurized autosampling for recovery of enhanced oil.

Theingi et al. [6] describe the planar five-bar linkage as planar manipulator using coupled kinematics in order to overcome the singularities. Alici et al. [7] presented several interesting polynomial approaches for solving the inverse kinematics (IK) equations of the five-bar linkage. Liu et al. [8] show the singularities for two situations that we also considered as boundary conditions for our research. The above-mentioned paper treated the singularity where the end-effectors of two neighboring elements are collinear or folded (B_1PB_2 as referred in this paper) and the situation when the two consecutive elements that neighbor the motor element in one direction (A_1B_1P or A_2B_2P as referred in this paper) are either

collinear or in a folded position. Consequently, we have to consider a transmission angle in the design between the elements of such a device to make sure that our mechanism will not get in a situation where the angle between two adjacent elements is equal to 0° (folded position) or 180° (extended position). In ref. [9], the same authors proposed a performance atlas to characterize the optimum design of the five-bar symmetrical parallel mechanism considering global conditioning index (GCI), the global velocity index, the global payload index, and the global stiffness index (GSI).

For a similar application as we intend to develop, Huang [10] analyzed the workspace of five-bar linkages and underlined the importance of avoiding singularities while maintaining the end-effector in the workspace area. The singularities are certain points in space where the mechanism becomes uncontrollable due to multiple solutions to the equation that describes the movement of the mechanism's elements, which brings the end-effector in the desired position. To quantify the relationship between the workspace and singularities, a dexterity index was defined. The optimum design was chosen between the design optimization carried out by the method of parametric variations and by the simplex direct search algorithm.

Campos [11] shows the development of a five-bar manipulator DexTAR with an optimized design with defined singularity-free zone inside the theoretical workspace. The previous work is further developed by Joubair [12] with the kinematic calibration of a five-bar planar parallel robot including all kinematic parameters and linearization of the model for each calibration configuration.

An interesting solution for motion between extreme points is demonstrated in the work done by Nafees et al. [13] by using dyadic and triadic concepts. Kiper et al. [14, 15] studied the synthesis of a planar five-bar mechanism by using the function generation synthesis with equal spacing and Chebyshev approximation, respectively, by using least squares approximation. In order to develop mechanisms with higher stiffness and low weight Kiper et al. [16] proposed, starting from a five-bar linkage, to develop a calibration method for an overconstrained six-bar linkage with 2 DoF. Although that it is a different application, Wang et al. [17] presented a solution to simplify a seven-bar linkage into a five-bar linkage but when it comes to dealing with the singularities of the mechanism a similar solution has been taken into account. One of the aspects that have to be connected with the singularities is the workspace and the workspace optimization in accordance with the presence of certain singularities. Yao et al. presented a paper where the workspace and orientation are studied, and singularities are considered so that the capability of the mechanism to be at its optimum [18].

Other works including [19, 20] briefly study the singularity of a five-bar linkage or a mechanism that can be transposed from a lower- or upper-class mechanism. Other research is oriented in the dimensioning of the DC motors of the five-bar linkage by Shengqi [21], in the development of control strategies of the planar 2 DoF manipulator by Roskam and Luc [22] and by Can and Sen [23] in minimizing the energy consumption through regenerative drives and optimally designed compliant elements.

The state of the art pointed out that an analytical synthesis for the five-bar linkage is missing from the literature, especially regarding the assurance of a singularity-free dexterous workspace and the lack of singularities inside of the total workspace. The current investigation proposes an analytical method for sizing the length of the links of the five-bar linkage of type 5-RRRRR resulted from the synthesis. To characterize the synthesized symmetrical five-bar structure, specific performance indices are computed and discussed. An experimental investigation on a prototype of the five-bar linkage with the structure 5-RRRRR validated the proposed analytical synthesis method.

2. Type synthesis of the five-bar linkage

The planar five-bar linkage contains (as the name suggests) a number of five elements ($n = 5$) and takes into account the relationship between the number of loops N :

$$N = \sum_{i=1}^2 e_i - n + 1, \quad (1)$$

Table I. Kinematic chains of the five-bar linkage.

5-RRRRR	5-RRRRR	5-RRRPP	5-RRPPP	5-RPPPP
	5-RRPRP	5-RPRPP		5-PPPPP

where e_i is the number of the kinematic pairs with DoF = i , $i = \{1, 2\}$. It results that for the number of loops $N = 1$, the number of the kinematic pairs are 5.

By considering the number of the kinematic pairs with DoF = 2, $e_2 = 0$, the mobility of the five-bar linkage, $M = 2$, results from the condition of the constrained motion, according to Alt [24]:

$$2(e_1 + e_2/2) - 3n + 3 + M = 0. \tag{2}$$

The number of elements of the five-bar linkage of different ranks can be computed from the diophantine equations system:

$$\begin{cases} n = n_2 + n_3 \\ 2 \sum_{i=1}^2 e_i = 2n_2 + 3n_3 \end{cases} \rightarrow \begin{cases} 5 = n_2 + n_3 \\ 10 = 2n_2 + 3n_3 \end{cases}. \tag{3}$$

where n_2, n_3 are the numbers of binary and ternary elements. The higher rank elements were neglected. The solution of the equations system gives the number of binary and ternary elements:

$$n_2 = 4, \quad n_3 = 0. \tag{4}$$

The possible kinematic chains of the five-bar linkage are shown in Table 1. Their number is 8. As shown in Table 1, some combinations were excluded, because they are identical with the previous ones.

By using the extended Franz von Reuleaux method, which consists of considering by turn one element as frame, two elements as drive and a fourth one as driven element for each kinematic chain, result all five-bar linkage configurations. The two elements jointed with the frame are chosen as the two drive elements. The full development of these five-bar linkages is shown in Fig. 1.

The number of the symmetrical five-bar linkages is limited to 8: 5-RRRRR(a), 5-RRRRP(c), 5-RRRPP(e), 5-RRPPP(b), 5-RPPPP(d), 5-PPPPP(a), 5-RRPRP(b), and 5-RPRPP(e). The symmetrical five-bar linkage structure that we consider forward is the 5-RRRRR(a) linkage (the frame element of the kinematic chain is written in the brackets). This structure is considered because the structure uses only revolute joints, which are easily manufactured with high precision, the elements have a symmetrical displacement, and they use only links with constant length. The size of the extended and folded 5-RRRRR(a) linkage shows to be favorable for the structure using only revolute joints. The five-bar linkages type 5-RRRRR(a) are actuated by two revolute servoactuators, which are fairly simple to control. The other symmetrical five-bar linkages use passive prismatic joints, which are more difficult to manufacture and operate properly. The linear actuators as active prismatic joints have a limited stroke and a large size in comparison with the revolute servo actuators.

3. Direct and IK of five-bar linkage 5-RRRRR(a)

The five-bar linkage 5-RRRRR(a) was chosen symmetrical to the vertical y-axis and the frame jointed elements 2 and 5, respectively, and the driven elements 3 and 4 are chosen equal ($l_2 = l_5, l_3 = l_4$). The drive elements are the elements 2 and 5, and the characteristic point M of the five-bar linkage is identical with the rotational joint C.

The kinematic schema of the symmetrical five-bar linkage 5-RRRRR(a) is shown in Fig. 2. The vectorial equations, written in complex numbers, for the two open loops OA_0BM and OE_0DM to the characteristic point M are

	Kinematic chain	Frame a	Frame b	Frame c	Frame d	Frame e
5 R R R R R R						
5 R R R R P						
5 R R R P P						
5 R R P P P						
5 R P P P P						
5 P P P P P						
5 R R R P P						
5 R P R P P						

Figure 1. Variety of the five-bar linkages as results of kinematic type synthesis and frame element selection.

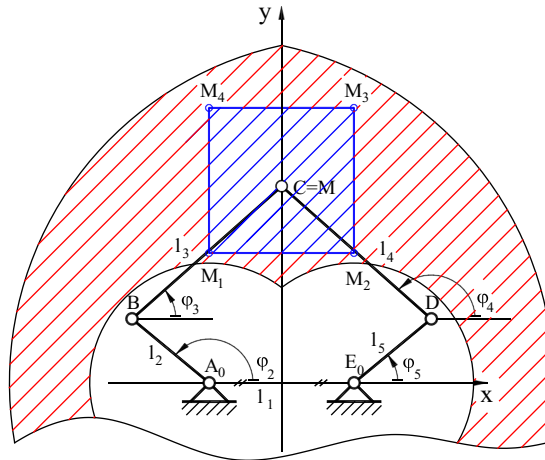


Figure 2. Kinematic schema of the symmetrical five-bar linkage.

$$\begin{aligned}
 M &= -\frac{l_1}{2} + l_2 e^{i\varphi_2} + l_3 e^{i\varphi_3}, \\
 M &= \frac{l_1}{2} + l_5 e^{i\varphi_5} + l_4 e^{i\varphi_4},
 \end{aligned}
 \tag{5}$$

where:

- $l_1, l_2, l_3, l_4 = l_3$ and $l_5 = l_2$ are the elements length of the five-bar linkage,
- $\varphi_2, \varphi_3, \varphi_4,$ and φ_5 are the positional angles of the elements in the reference system.

3.1. Direct kinematic

The transmission equations based on the passive angles φ_3 or φ_4 with respect to the drive angles φ_2 and φ_5 used for direct kinematic result in the form:

$$\begin{aligned}
 0 &= A_3(\varphi_2, \varphi_5) \cos \varphi_3 + B_3(\varphi_2, \varphi_5) \sin \varphi_3 + C_3(\varphi_2, \varphi_5), \\
 0 &= A_4(\varphi_2, \varphi_5) \cos \varphi_4 + B_4(\varphi_2, \varphi_5) \sin \varphi_4 + C_4(\varphi_2, \varphi_5).
 \end{aligned}
 \tag{6}$$

where:

$$\begin{aligned}
 A_3(\varphi_2, \varphi_5) &= -2l_3[l_1 + l_2(\cos \varphi_5 - \cos \varphi_2)], \quad B_3(\varphi_2, \varphi_5) = -2l_2l_3(\sin \varphi_5 - \sin \varphi_2), \\
 C_3(\varphi_2, \varphi_5) &= l_1^2 - 2l_1l_2(\cos \varphi_5 - \cos \varphi_2) - 2l_2^2(1 + \cos(\varphi_5 - \varphi_2)), \\
 A_4(\varphi_2, \varphi_5) &= 2l_3[l_1 + l_2(\cos \varphi_5 - \cos \varphi_2)], \quad B_4(\varphi_2, \varphi_5) = 2l_2l_3(\sin \varphi_5 - \sin \varphi_2), \\
 C_4(\varphi_2, \varphi_5) &= l_1^2 - 2l_1l_2(\cos \varphi_5 - \cos \varphi_2) - 2l_2^2(1 - \cos(\varphi_5 - \varphi_2)),
 \end{aligned}
 \tag{7}$$

The positional passive angles φ_3 or φ_4 are calculated with the relationship:

$$\varphi_i(\varphi_2, \varphi_5) = 2 \cdot \arctan \frac{B_i(\varphi_2, \varphi_5) \mp \sqrt{A_i^2(\varphi_2, \varphi_5) + B_i^2(\varphi_2, \varphi_5) - C_i^2(\varphi_2, \varphi_5)}}{A_i(\varphi_2, \varphi_5) - C_i(\varphi_2, \varphi_5)}, \quad i = 3, 4.
 \tag{8}$$

The coordinates of the characteristic point $M(x_M, y_M)$ result from the relationships (5) as follows:

$$\begin{aligned}
 x_M &= -\frac{l_1}{2} + l_2 \cdot \cos \varphi_2 + l_3 \cdot \cos \varphi_3, & y_M &= l_2 \cdot \sin \varphi_2 + l_3 \cdot \sin \varphi_3, \\
 x_M &= +\frac{l_1}{2} + l_5 \cdot \cos \varphi_5 + l_4 \cdot \cos \varphi_4, & y_M &= l_5 \cdot \sin \varphi_5 + l_4 \cdot \sin \varphi_4.
 \end{aligned}
 \tag{9}$$

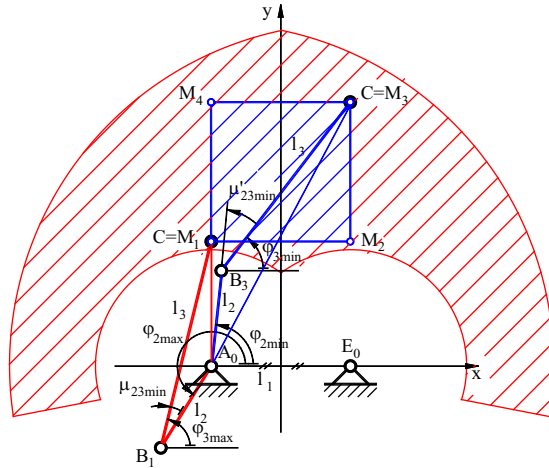


Figure 3. Dimensional conditions in order to avoid collinearity positions of elements 2 and 3.

3.2. Inverse kinematic

The transmission equations based on the drive angles φ_2 and φ_5 and the coordinates of the characteristic point $M(x_M, y_M)$ used for IK result in the form:

$$\begin{aligned}
 F_2(x_M, y_M) &= A_2(x_M, y_M) \cos \varphi_2 + B_2(x_M, y_M) \sin \varphi_2 + C_2(x_M, y_M) = 0 \\
 F_5(x_M, y_M) &= A_5(x_M, y_M) \cos \varphi_5 + B_5(x_M, y_M) \sin \varphi_5 + C_5(x_M, y_M) = 0
 \end{aligned}
 \tag{10}$$

where the coefficients are

$$\begin{aligned}
 A_2(x_M, y_M) &= -l_2(2x_M + l_1) & B_2(x_M, y_M) &= -2l_2y_M \\
 C_2(x_M, y_M) &= x_M^2 + y_M^2 + \frac{l_1^2}{4} + l_2^2 - l_3^2 + l_1x_M
 \end{aligned}
 \tag{11}$$

$$\begin{aligned}
 A_5(x_M, y_M) &= -l_5(2x_M - l_1) & B_5(x_M, y_M) &= -2l_5y_M \\
 C_5(x_M, y_M) &= x_M^2 + y_M^2 + \frac{l_1^2}{4} + l_5^2 - l_4^2 - l_1x_M
 \end{aligned}
 \tag{12}$$

The positional angles of the drive elements are calculated according to the relationship:

$$\varphi_i(x_M, y_M) = 2 \cdot \arctan \frac{B_i(x_M, y_M) \mp \sqrt{A_i^2(x_M, y_M) + B_i^2(x_M, y_M) - C_i^2(x_M, y_M)}}{A_i(x_M, y_M) - C_i(x_M, y_M)}, \quad i = 2, 5 \tag{13}$$

4. Synthesis of symmetrical five-bar linkage 5-RRRRR(a)

The synthesis of the symmetrical five-bar linkage 5-RRRRR(a) allows the computing of the length of the elements so that the characteristic point M moves inside the dexterous workspace, which belongs to the total workspace (see Fig. 2) and it should be singularity-free. The dexterous workspace is chosen with a square or rectangular geometry, which is more appropriate for applications mentioned before.

For this condition, it is necessary to avoid the collinearity (folded or extended) of the mobile neighboring links (see Figs. 3 and 4). The collinearity conditions are identical for both open loops OA_0BM and OE_0DM , because of the symmetrical design. That means the drive element 2 and the driven element 3, respectively the drive element 5 and the driven element 4, should avoid the folded and extended positions. Between the drive and driven elements, there is an input transmission angle corresponding to the collinearity position (μ_{23} and μ'_{23}).

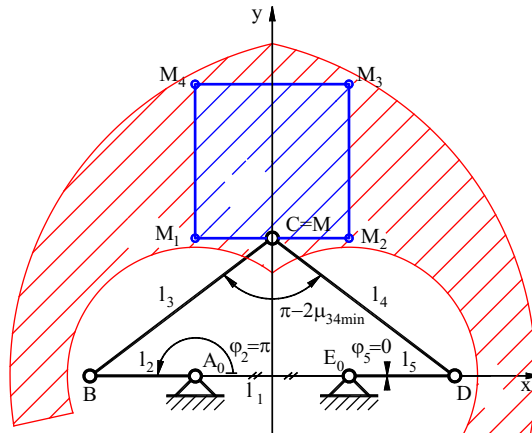


Figure 4. Dimensional conditions in order to avoid collinearity positions of elements 3 and 4.

The folded position can be avoided if the normal length from the drive joint A_0 and the border of the dexterous workspace is bigger than the difference of the lengths of the elements 2 and 3 (see Fig. 3). The analytical condition is given by the relationship:

$$y_{M1} \geq |l_2 - l_3|. \tag{14}$$

The extended position can be avoided if the distance from the drive joint A_0 to the farthest point M_3 is lower than the sum of the length of the elements 2 and 3 (see Fig. 3). The analytical condition is given by the relationship:

$$\sqrt{(x_{M3} + l_1/2)^2 + y_{M3}^2} \leq l_2 + l_3. \tag{15}$$

The condition to avoid the extended position between the driven elements 3 and 4, which means also to change the side of the characteristic point toward the frame joint line, consists in having the sum of the frame and the drive length of the elements lower than the sum of the driven elements (see Fig. 4). The analytical condition is given by the relationship:

$$l_1 + 2l_2 \leq 2l_3. \tag{16}$$

If the three conditions given by the inequations (14), (15), and (16) are fulfilled, the dexterous workspace is singularity-free. To have an analytical solution of the synthesis, each inequation from the inequation system will be substituted through an equation, by imposing a coefficient $k > 1$. In this case, the substituted equation system can be written in the form:

$$l_2 + l_3 = k\sqrt{(x_{M3} + l_1/2)^2 + y_{M3}^2} \tag{17}$$

$$k(l_3 - l_2) = y_{M1} \tag{18}$$

$$kl_1 + 2l_2 = 2 \cdot l_3 \tag{19}$$

The coefficient k multiplied with the lower side of each inequation ensures the avoidance of the collinearity positions of the mobile neighboring elements. Also, that means the existence of an input or an output transmission angle between the neighboring elements and, of course, a singularity-free dexterous workspace.

Table II. Coordinates of the corner points of the square dexterous workspace.

Corner points	x_M [mm]	y_M [mm]
M_1	-100	130
M_2	100	130
M_3	100	330
M_4	-100	330

Table III. Computed elements length.

Number of the element	Symbol	Length [mm]
1	l_1	154
2	l_2	194
3	l_3	294
4	l_4	294
5	l_5	194

The solutions of the substituted equations system are the elements lengths, as follows:

$$l_1 = 2y_{M1}/k^2, \tag{20}$$

$$l_2 = \frac{1}{2} \left(k\sqrt{(x_{M3} + l_1/2)^2 + y_{M3}^2} - \frac{1}{k}y_{M1} \right), \tag{21}$$

$$l_3 = \frac{1}{2} \left(k\sqrt{(x_{M3} + l_1/2)^2 + y_{M3}^2} + \frac{1}{k}y_{M1} \right). \tag{22}$$

Considering the symmetry conditions, the length of the elements is

$$l_4 = l_3, l_5 = l_2. \tag{23}$$

If a minimum input transmission angle $\mu_{23\min}$ is required, the coefficient k can be computed from the triangle $A_0B_1M_1$ (see Fig. 3) with the relationship:

$$y_{M1}^2 = l_2^2 + l_3^2 - 2l_2l_3\cos \mu_{23\min}, \tag{24}$$

in the form:

$$k = \sqrt{\frac{y_{M1}^2 - \sqrt{y_{M1}^4 - \left[(x_{M3} + \frac{l_1}{2})^2 + y_{M3}^2 \right] y_{M1}^2 (1 - (\cos \mu_{23\min})^2)}}{\left[(x_{M3} + \frac{l_1}{2})^2 + y_{M3}^2 \right] (1 - \cos \mu_{23\min})}}, \tag{25}$$

5. Performances analysis of the symmetrical five-bar linkage 5-RRRRR(a)

The characterization of the kinematic performances of the symmetrical five-bar linkage is done for a given square dexterous workspace and with the length of the elements computed with the analytical relationships (20)–(22). The dexterous workspace is defined through the corner points $M_1, M_2, M_3,$ and $M_4,$ given in Table 2.

For a required minimum transmission angle of $\mu_{23\min} = 20^\circ,$ the computed coefficient with the relationship (25) is $k = 1, 3$ and the elements lengths computed with the relationships (20)–(23) are given in Table 3.

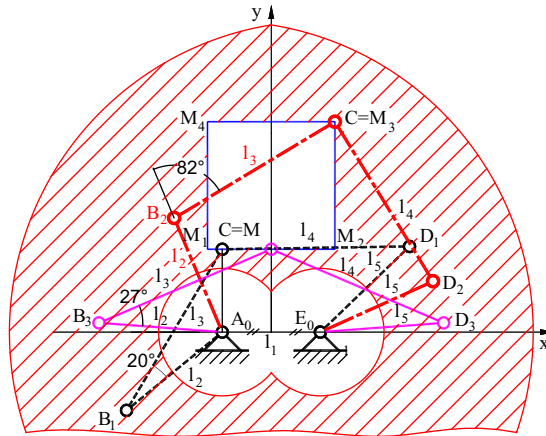


Figure 5. Kinematic schema with the synthesized five-bar linkage in the critical positions.

The kinematic schema shows the symmetrical five-bar linkage in the critical positions (see Fig. 5). It is shown that in all critical positions, the transmission angle is $\mu_{1\min} \geq 20^\circ$. All other positions inside the dexterous workspace fulfill the condition imposed to the transmission angle.

5.1. Singularities of type I

The singularities of type I are positions of the characteristic point M in the dexterous workspace with the property that by actuating the drive elements, the characteristic point does not move. The vector of input parameters of the five-bar linkage is $Q = [\varphi_2, \varphi_5]^T$ and the vector of the output parameters is $X = [x_M, y_M]^T$. For this case, the singular positions can be determined by finding the zero values of Jacobian matrix determinant $\det(J_q)$ [25–29]:

$$\det(J_q) = \begin{vmatrix} \frac{\partial F_2(X, Q)}{\partial \varphi_2} & \frac{\partial F_2(X, Q)}{\partial \varphi_5} \\ \frac{\partial F_5(X, Q)}{\partial \varphi_2} & \frac{\partial F_5(X, Q)}{\partial \varphi_5} \end{vmatrix} = 0, \tag{26}$$

where

$$\frac{\partial F_2(X, Q)}{\partial \varphi_2} = -A_2(x_M, y_M) \sin \varphi_2 + B_2(x_M, y_M) \cos \varphi_2, \quad \frac{\partial F_2(X, Q)}{\partial \varphi_5} = 0, \tag{27}$$

$$\frac{\partial F_5(X, Q)}{\partial \varphi_2} = 0, \quad \frac{\partial F_5(X, Q)}{\partial \varphi_5} = -A_5(x_M, y_M) \sin \varphi_5 + B_5(x_M, y_M) \cos \varphi_5. \tag{28}$$

Figure 6a shows that the singularities of type I are avoided in the whole dexterous workspace, while any zero values of the Jacobian matrix determinant J_q are to be reported. The minimum value of $\det(J_q)$ is $-2.76 \cdot 10^9 \text{ mm}^4$.

5.2. Singularities of type II

The singularities of type II are positions of the characteristic point M in the dexterous workspace with the property that by non-actuated drive elements the characteristic point allows an infinitesimal motion. For this case, the singularity positions can be computed for zero values of Jacobian matrix determinant $\det(J_x)$ [25–29]:

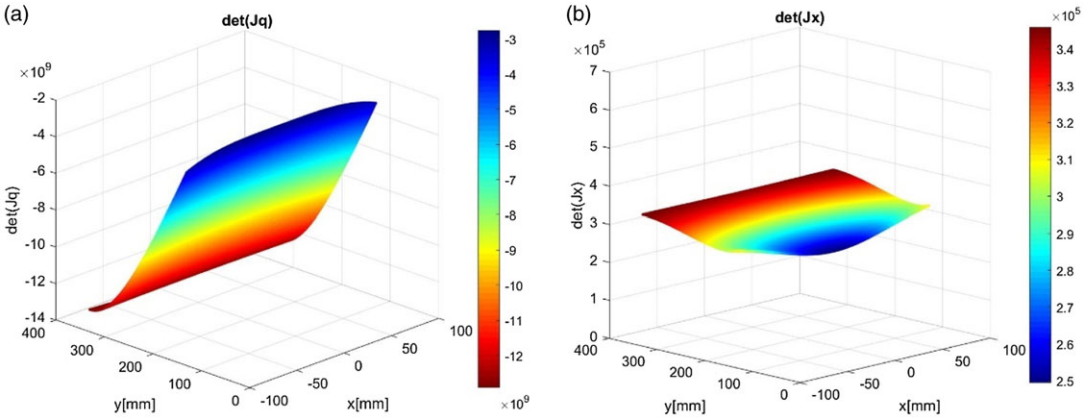


Figure 6. Singularities of type I (a) and type II (b) analysis in the whole dexterous workspace.

$$\det(J_x) = \begin{vmatrix} \frac{\partial F_2(X, Q)}{\partial x_M} & \frac{\partial F_2(X, Q)}{\partial y_M} \\ \frac{\partial F_5(X, Q)}{\partial x_M} & \frac{\partial F_5(X, Q)}{\partial y_M} \end{vmatrix} = 0, \tag{29}$$

where

$$\frac{\partial F_2(X, Q)}{\partial x_M} = -2l_2 \cos \varphi_2 + 2x_M + l_1, \quad \frac{\partial F_2(X, Q)}{\partial y_M} = -2l_2 \sin \varphi_2 + 2y_M, \tag{30}$$

$$\frac{\partial F_5(X, Q)}{\partial x_M} = -2l_5 \cos \varphi_5 + 2x_M - l_1, \quad \frac{\partial F_5(X, Q)}{\partial y_M} = -2l_5 \sin \varphi_5 + 2y_M. \tag{31}$$

Figure 6b shows that the Jacobian matrix determinant J_x is not equal to zero, which means the dexterous workspace is free of singularities of type II. The minimum value of $\det(J_x)$ is $2.5 \cdot 10^5 \text{ mm}^2$.

5.3. Manipulability indices

The local manipulability index (LMI) is defined as absolute value of the determinant of the Jacobian matrix J given by the relationship:

$$\mu = |\det J| = |\det(J_x J_q^{-1})|, \tag{32}$$

mentioning that the relationship is valid for redundant manipulators [25–29].

The normalized values of the LMIs are determined as min-max feature scaling. The normalized values of the LMIs are non-dimensional and in the same range [0.27, 1] (see Fig. 7).

The region of the dexterous workspace closer to the actuated joints has a higher manipulability value than the furthest regions as shown in Fig. 7a and b.

The global measure of the manipulability global manipulability index (GMI) in the dexterous workspace W can be computed with the relationship:

$$\text{GMI} = \frac{\int_w \mu dw}{\int_w dw}, \tag{33}$$

and the value for the considered dexterous workspace of the five-bar linkage is given in Table 4.

The value of GMI of 0.5742 shows that it is close to the best value of 1, which is the favorable measure of manipulability.

Table IV. Global manipulability index (GMI).

5-RRRRR(a)	GMI	0.5742
------------	-----	--------

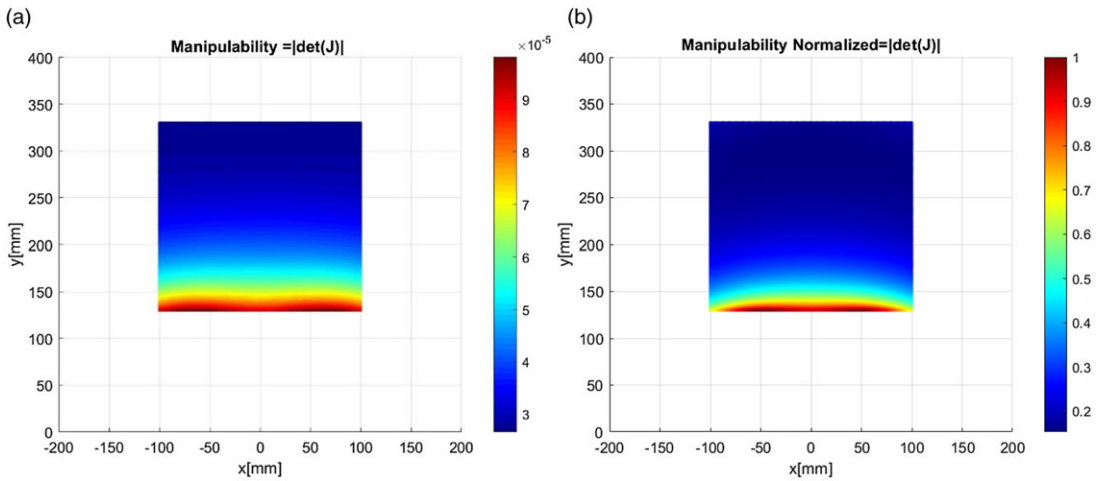


Figure 7. The computed local manipulability indices (a) and normalized manipulability indices of the five-bar linkage (b).

5.4. Condition number

The Jacobian condition number is a measure of dexterity and accuracy of a manipulator. It is defined as the product between the norms of Jacobian matrix and inverse Jacobian matrix given by the relationship:

$$k = \|J\| \|J^{-1}\|. \tag{34}$$

Because the Jacobian condition number takes values in the range $[1, +\infty]$, it is preferable to use the inverse value of the condition number, which has values in the range $[0, 1]$. This inverse Jacobian conditional number is known as local conditional index LCI and is given by the relationship [27–30]:

$$LCI = \frac{1}{k}. \tag{35}$$

The values of the condition numbers are favorable because the most values are close to 1, only the right-side corner shows not favorable values, but even this LCI values are higher than 0.3127 (see Fig. 8a and b), which means the synthesized five-bar linkage has a high dexterity inside the dexterous workspace.

The GCI can be obtained by computing the local conditioning index over the dexterous workspace with the relationship:

$$GCI = \frac{\int_w \frac{1}{k} dw}{\int_w dw}. \tag{36}$$

The kinematic condition index (KCI) measures the performance of a manipulator given by the relationship:

$$KCI = \frac{1}{k_{\min}} \cdot 100\%. \tag{37}$$

The computed values of the GMI and KCI are given in Table 5. The value of the GMI is closer to 1, which means that small changes in input produce small changes in output and the Jacobian matrix is well conditioned. The value of 99.05 % for the KCI is very favorable.

Table V. Global conditioning index (GCI) and kinematic condition index (KCI).

5-RRRRR(a)	GCI	0.6423
5-RRRRR(a)	KCI	99.05%

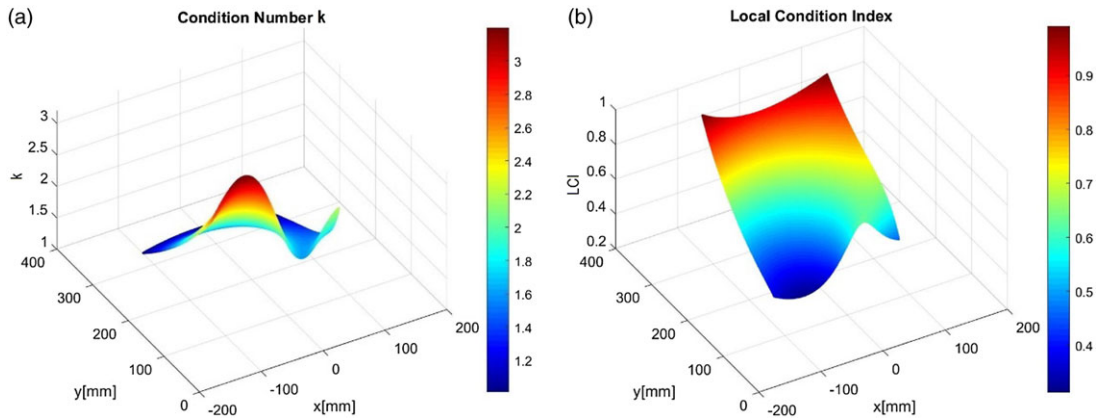


Figure 8. The computed condition number (a) and local condition index (b) of the five-bar linkage.

5.5. Stiffness index

The local stiffness index, which depends on multiple parameters (geometry, material, actuators, mechanisms), is analytically defined as inverse of the conditional number of the stiffness matrix:

$$\eta_k = 1 / (\|K\| \|K^{-1}\|), \tag{38}$$

with the stiffness matrix given as product between the scalar value $k \in [0, 1]$, which indicate the stiffness of each actuator, the transposed Jacobian matrix, and the Jacobian matrix [28–29, 31]:

$$K = kJ^T J, \tag{39}$$

Figure 9 shows the map of the local stiffness indices with values in the range of [0.0098, 0.9811]. The most values of LSI are favorable, higher than 0.4, without the values of the right-side corner of the map, which are in closer regions to the drive joints.

The GSI in the dexterous workspace is computed as mean value with the relationship:

$$GSI = \frac{\int_w \eta_k dw}{\int_w dw}. \tag{40}$$

The GSI of 0.4366 has a value closer to the middle value of the LSI range, meaning a good stiffness of the five-bar linkage.

5.6. Power transmission indices

The transmission angle, which characterizes the efficiency of power transmission from the input to the output link, gives three types of transmission indices [32–35]:

- Input transmission index (ITI):

$$ITI = \min(|\cos \mu_{23}|, |\cos \mu_{54}|), \tag{41}$$

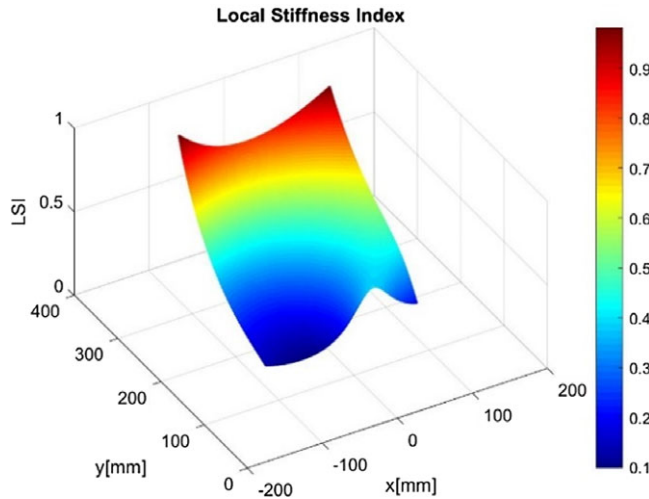


Figure 9. The computed local stiffness indices of the five-bar linkage.

where μ_{23}, μ_{54} are the transmission angles between the input links (1) and (5) and the next connected links (3), respectively (4).

- Output transmission index (OTI):

$$OTI = \min(|\cos \mu_{34}|), \tag{42}$$

where μ_{34} is the transmission angle between the output mobile links (3) and (4).

- Local transmission index (LTI):

$$LTI = \min(ITI, OTI) . \tag{43}$$

The transmission angles μ_{23} and μ_{54} can be computed from the triangles A_0BM and E_0DM , where $C = M$ as (see Fig. 3):

$$\mu_{23} = \arccos \frac{l_2^2 + l_3^2 - [(x_M + l_1/2)^2 + y_M^2]}{2l_2l_3} \quad \mu_{54} = \arccos \frac{l_4^2 + l_5^2 - [(x_M - l_1/2)^2 + y_M^2]}{2l_4l_5} \tag{44}$$

and the transmission angle μ_{34} results from the triangles A_0BM , E_0DM , and A_0ME_0 as (see Fig. 4):

$$\mu_{34} = \widehat{A_0MB} + \widehat{A_0MB_0} + \widehat{DME_0}, \tag{45}$$

$$\widehat{A_0MB} = \arccos \frac{l_3^2 + [(x_M + l_1/2)^2 + y_M^2] - l_2^2}{2l_3\sqrt{[(x_M + l_1/2)^2 + y_M^2]}}, \tag{46}$$

$$\widehat{A_0MB_0} = \arccos \frac{[(x_M + l_1/2)^2 + y_M^2] + [(x_M - l_1/2)^2 + y_M^2] - l_1^2}{2\sqrt{[(x_M + l_1/2)^2 + y_M^2]}\sqrt{[(x_M - l_1/2)^2 + y_M^2]}}, \tag{47}$$

$$\widehat{DME_0} = \arccos \frac{l_4^2 + [(x_M - l_1/2)^2 + y_M^2] - l_5^2}{2l_4\sqrt{[(x_M - l_1/2)^2 + y_M^2]}}. \tag{48}$$

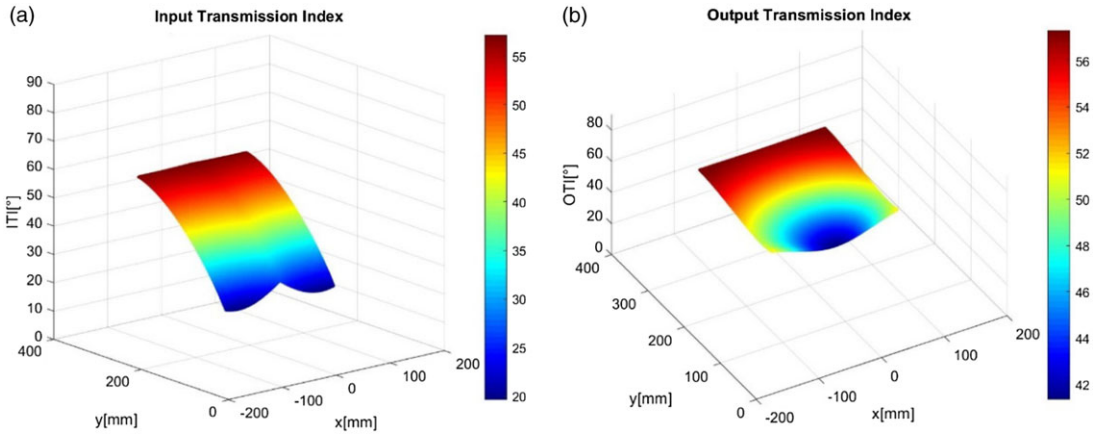


Figure 10. The computed input (a) and output (b) transmission indices of the five-bar linkage.

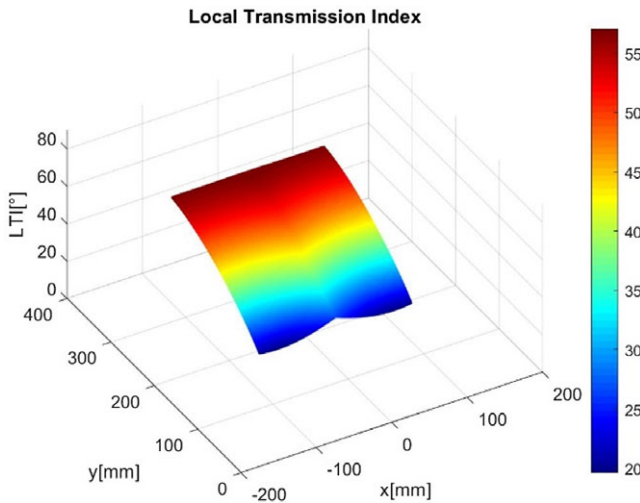


Figure 11. The computed local transmission index of the five-bar linkage.

Figure 10a shows the map of the ITI expressed in degrees. The values of ITI are in the range of $[19.62, 57.10]^\circ$ or expressed in radians $[0.3425, 0.9967]$ rad, with good efficiency of power transmission. As expected, the minimum value of the transmission angle is 19.62° , very close to the imposed value of 20° . The ITIs are symmetrically distributed in respect of the y-axis of the dexterous workspace, with the lower values close to the lower border of the workspace and the higher values close to the upper border.

Figure 10b shows the map of the OTI in 3D representations. The values of OTI are included in the range of $[41.34, 57.29]^\circ$ or expressed in radians $[0.7216, 0.9999]$ rad. The values of the OTI are symmetrically distributed in respect of the y-axis of the dexterous workspace, with the lower values situated in the origin of the cartesian axes system and the higher values on the upper side corners.

The local transmissibility index is identical with the ITI (see Fig. 11).

The global values of ITI, OTI, and LTI in the dexterous workspace can be computed with the relationships (Tables 6 and 7):

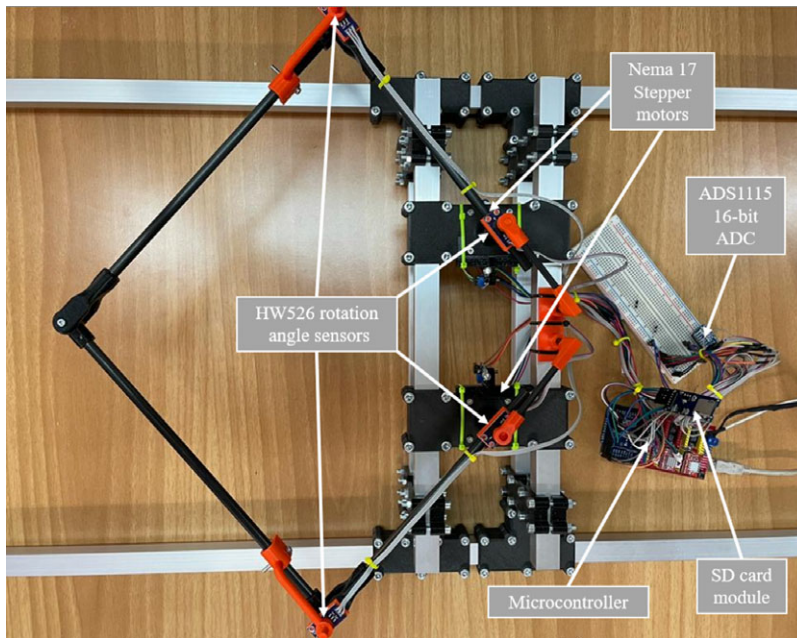
$$GITI = \frac{\int_w ITI \cdot dw}{\int_w dw}, \quad GOTI = \frac{\int_w OTI \cdot dw}{\int_w dw}, \quad GLTI = \frac{\int_w LTI \cdot dw}{\int_w dw}. \quad (49)$$

Table VI. Global stiffness index (GSI).

5-RRRRR(a)	GSI	0.4366
------------	-----	--------

Table VII. Global input, output, and local transmissibility index GITI, GOTI, and GLTI.

5-RRRRR(a)	GITI	0.7575 rad	43.40°
5-RRRRR(a)	GOTI	0.8929 rad	51.16°
5-RRRRR(a)	GLTI	0.7575 rad	43.40°

**Figure 12.** Experimental stand with planar five-bar linkage.

6. Applications of design solution for 3D printer design

The test stand consists of a frame built with square aluminum tubes and 3D printed parts. By means of some 3D printed supports, onto the frame was fastened the stepper motors that actuate the drive elements of the five-bar linkage. The linkage was designed to have 3D printed joints and carbon fiber round tubes as cranks (Fig. 12).

To control the electronics, we used a combination of Arduino platform with IR distance sensors (used to “Home” the mechanism into a known position) and a set of accelerometers to read the yaw angles of the secondary linkage. The computer works as a programming interface for the microcontroller that controls the linkage by means of the stepper motors and the accelerometers working as an encoder to read out the angle values. This cycle repeats itself for a given number of times so the angle values are known at every position.

The hardware chosen for the implementation of the control sequence and data acquisition is as follows: a development board based on the ATmega2560 microcontroller (Arduino Mega 2560), two A4988 stepper motor drivers, two HW201 IR proximity sensors, four HW526 rotation angle sensor modules, an ADS1115 4 Channel 16-bit ADC, and a MicroSD card Adapter (Fig. 12).

The architecture of the custom control software is developed based on the solution of the IK which is used to compute the required angular position of the actuated links with respect to an imposed set of cartesian coordinates for the characteristic point of the end-effector. In this manner, a function was implemented in order to compute the previously mentioned angular positions.

Regarding the motion control algorithm, the chosen approach was to compute the linear trajectory between an imposed cartesian coordinate set, representing the destination of the movement, and the current cartesian position, followed by a division in smaller segments, along the linear trajectory.

Using the function for solving the driven links angles for each point along the imposed trajectory, the required angular positions are obtained and by subtracting the values between each two consecutive pair of points along the imposed trajectory, the required variation for each actuated link is obtained.

Computing the required number of steps of each stepper motor is achieved from the previously mentioned variance by transforming the angular value from radians to degrees and compensating for the step angle of the stepper motor to reach each intermediate point along the imposed trajectory. The number of steps required for the movement between each interval obtained as previously presented will most likely represent non-integer numbers, thus resulting in a necessary rounding of the values. The error generated by the rounding operation is saved and carried over to the next intervals of motion and is compensated if it overcomes a step or if it becomes negative by adding or subtracting a step from the current motion.

Regarding the actuation of the stepper motors, the previously computed step values are required to be executed by both stepper motors in the same over-all time of motion. Given the fact that the microcontroller used is an ATmega2560, which is not able of multithreading, it is not possible to execute tasks in parallel sequences; thus, the closest approach is to execute the pulses in a cross-pattern between each stepper motor. This approach is not useful since the steps required for the movement of the two actuated links have different values most of the time. To solve this issue, the number of divisions among the imposed trajectory is increased to such an extent that the resulting number of pulses in each segment, after rounding, becomes either 0 or 1. This approach is very inefficient performance-wise, resulting in a limitation of the maximum speed of the end-effector. The maximum speed limitation with the microcontroller used (ATmega2560) is approximately 0.3 m/s.

The control algorithm also requires an initialization sequence since the IKP solving function outputs absolute coordinates based on absolute cartesian coordinates of the end-effector. The initialization sequence is implemented by moving the actuated link in an imposed direction until the two HW201 IR proximity sensors are triggered, thus homing the mechanism and setting a fixed reference system for the control algorithm.

After the successful implementation of the control sequence, it was desired to compare the experimental results to the theoretic counterpart with regard to the over-all movement of the linkage; thus, four HW526 rotation angle sensor modules were mounted on the drive and driven joints and the absolute angle of the drive joints and the relative angle of the driven joints were determined by using an ADS1115 4 Channel 16-bit ADC and saved on a .txt file on a MicroSD memory card, followed by the comparison to the theoretical results. The experimental test consists in the movement of the characteristic point of the square border of the dexterous workspace, as shown in Fig. 13.

Figure 13 shows the experimental and theoretical path of the described dexterous workspace path of the characteristic point M, and Fig. 14 describes the experimental and theoretical results of the drive, driven, and transmission angles of the five-bar linkage. The experimental results confirm that the followed path resembles the theoretical imposed one, with a maximum deviation of the characteristic point of $\varepsilon = 2$ mm. The same behavior of the experimental angle values can be highlighted. By comparing the experimental results and the theoretical counterpart, multiple issues can be observed. The behavior of the control algorithm is observed, that resulted from the rounding required for the stepper motors actuation, then, the presence of a certain level of misalignments or geometrical flaws is seen from the deflection of the plotted profile, and the presence of inertia, from the deflection in the regions representing the change in movement direction.

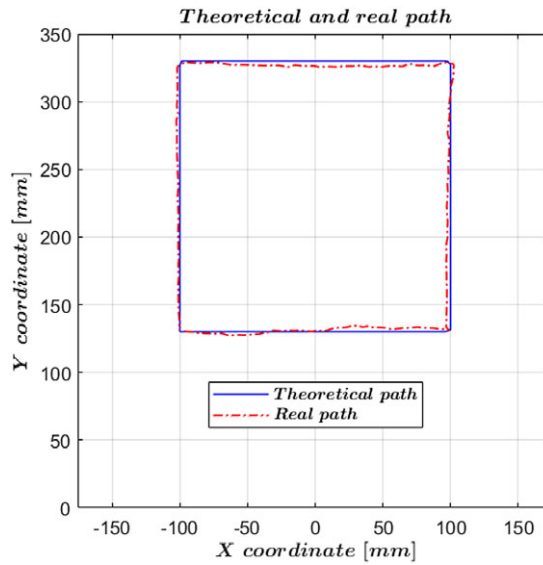


Figure 13. Experimental and theoretical path of the described dexterous workspace of the characteristic point *M*.

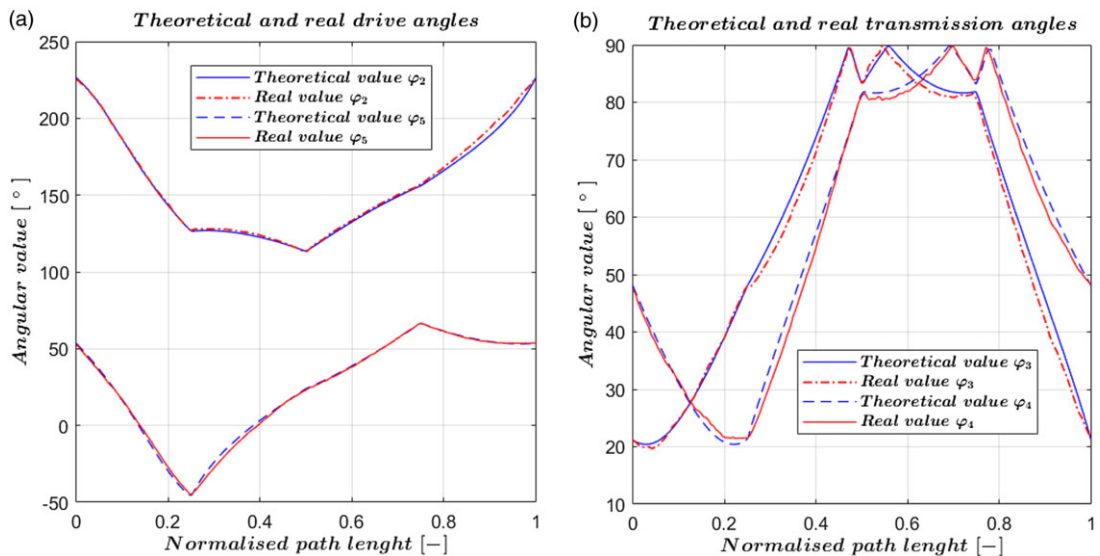


Figure 14. Experimental and theoretical results of the drive (a), driven (b), and transmission angles.

7. Conclusions

This paper shows a study starting with the structural synthesis, forward and IK analysis, dimensional synthesis, performance indices characterization, and experimental tests of the five-bar linkage.

The structural synthesis highlighted a number of eight useful five-bar linkage structures, which can be considered as symmetrical structures. This paper focused on the five-bar linkage 5-RRRRR(a) and proposed the direct and IK to compute further the performance indices and to use for the control of the experimental stand.

The main contribution of this paper was concentrated in the development of a dimensional synthesis of the five-bar linkage to avoid the singularities in a dexterous workspace defined by the user. The method allows the computing of all the elements length with analytical relationships by using a coefficient k . This coefficient can be further computed by imposing a minimum transmission angle in the worst positions of the workspace, which are the shorter distance between the frame joint and the lower border of the dexterous workspace.

To confirm the theoretical synthesis results, the Jacobian matrix determinant J_q and J_x were computed for a numerical example, confirming the nonexistence of zero values, which means the dexterous workspace is singularity-free of type I and II. Further for the characterization of the five-bar linkage, the local and global performance indices were computed such as manipulability index, conditional number (dexterity index), local condition index, local stiffness index, respectively the ITI, OTI, and LTI. Several characteristics of the performance indices were highlighted based on the considered numerical example.

For certifying the theoretical synthesis results, an experimental stand of the five-bar linkage was developed, and the tests results showed that the characteristic point describes the square border of the dexterous workspace, which means all other points inside of the dexterous workspace can be reached without having any type of singularities. The experimental path described by the characteristic point resembles the theoretical counterpart while the experimental values of the characteristic drive, driven, and transmission angles are very close to the theoretical ones, even though some control and calibration improvements are still required for the future research.

Acknowledgments. The authors would like to thank the Organizing Committee of IFIT 2022 for selecting the earlier paper for an extended paper version.

Authors' contributions. DT, LE, and SC conceived and designed the study; DT, LE, CM, and OA wrote the article; DT, LE, SC, and CM developed the mathematical model; LE, LA, and SD developed the performance characterization program; DT and SD realized the five-bar linkage prototype; DT, LE, and OA developed the experimental data acquisition and processing.

Financial support. This research received no specific grant from any funding agency, commercial, or not-for-profit sectors.

Competing interests. The authors declare no competing interests exist.

Ethical approval. Not applicable.

References

- [1] I. Tempea, M. Neacşa and A. Livadariu, "A New Acting Solution of a Double SCARA Robot," *In: Proceedings of the 3rd International Conference on "Computational Mechanics and Virtual Engineering" COMEC 2009, Brasov* (2009) pp. 765–770.
- [2] D. Tsetserukou, S. Hosokawa and K. Terashima, "LinkTouch: A Wearable Haptic Device with Five-Bar Linkage Mechanism for Presentation of Two-DOF Force Feedback at the Fingerpad," *In: Proceedings of IEEE Haptics Symposium, Houston* (2014) pp. 307–312.
- [3] W. W. Marzouk and A. R. Ahmed, "Analytical Model for Novel Design of Five-Bar Polycentric Knee Joint," *In: Proceedings of Conference: International Conference on Pure and Applied Sciences (ICPAS 2015), Luxor* (2015) pp. 1–13.
- [4] K. Sun, R. Ge, T. Li and J. Wang, "Design and analysis of vegetable transplanter based on five-bar mechanism," *IOP Conference Series: Materials Science and Engineering* **692**, 012029 (2019).
- [5] S. Jian, "The Research of Five-Bar Robot for Pressurized Autosampling for Enhanced Oil Recovery Research. *Master Degree Thesis* (St. John's, Newfoundland, Canada, 2016).
- [6] C. L. Theingi, I.-M. Chen and J. Angeles, "Singularity Management of 2DOF Planar Manipulator Using Coupled Kinematics," *In: Seventh International Conference on Control, Automation, Robotics and Vision (ICARCV'02), Singapore* (2002) pp. 402–407.
- [7] G. Alici, "An inverse position analysis of five-bar planar parallel manipulators," *Robotica* **20**(2), 195–201 (2002).
- [8] X.-J. Liu, J. Wanga and G. Pritschow, "Performance atlases and optimum design of the planar 5R symmetrical parallel mechanisms," *Mech. Mach. Theory* **41**(2), 119–144 (2006).
- [9] X.-J. Liu, J. Wanga and G. Pritschow, "Kinematics, singularity, and workspace of planar 5R symmetrical parallel mechanisms," *Mech. Mach. Theory* **41**(2), 145–169 (2006).

- [10] M. Huang, "Design of a planar parallel robot for optimal workspace and dexterity," *Int. J. Adv. Robot. Syst.* **8**(4), 176–183 (2011).
- [11] L. Campos, F. Bourbonnais, I. A. Bonev and P. Bigras, "Development of a Five-Bar Parallel Robot with Large Workspace," **In: Proceedings of the ASME 2010 International Design Engineering Technical Conferences & Computers and Information in Engineering Conference IDETC/CIE 2010**, Montreal, Quebec (2010) pp. 917–922.
- [12] A. Joubair, M. Slamani and I. A. Bonev, "Kinematic calibration of a five-bar planar parallel robot using all working modes," *Robot. Comput. Integr. Manuf.* **29**(4), 15–25 (2013).
- [13] K. Nafees and A. Mohammad, "Dimensional synthesis of a planar five-bar mechanism for motion between two extreme positions," *Aust. J. Mech. Eng.* **16**(1), 74–81 (2017).
- [14] G. Kiper, T. Bilginca and M. İ. C. Can, "Function generation synthesis of planar 5R mechanism," *Probl. Mech.* **51**(2), 28–31 (2013).
- [15] G. Kiper, B. Bağdadioglu and T. Bilginca, "Function Synthesis of the Planar 5R Mechanism Using Least Squares Approximation," **In: Advances in Robot Kinematics** (J. Lenarcic and O. Khatib, eds.) (Springer, Cham, 2014) pp. 69–76.
- [16] G. Kiper, M. İ. C. Dede, E. Uzunoglu and E. Matar, "Use of Hidden Robot Concept for Calibration of an Over-Constrained Mechanism," **In: Proceedings of the 14th IFToMM World Congress**, Taipei, Taiwan, October 25–30, 2015, vol. 4 (2015) pp. 243–247.
- [17] J. Wang, D. Z. L. Nie, J. Ren, Q. Wang and J. Sun, "Equivalent Five-bar Linkages for the Singularity Analysis of Two-DOF Seven-Bar Linkages," **In: Proceedings of ASME 2017 International Design Engineering Technical Conferences and Computers and Information in Engineering Conference, DETC2017-67527**, Cleveland, OH (2017).
- [18] W. Yao and J. S. Dai, "Workspace and orientation analysis of a parallel structure for robotic fingers," *J. Adv. Mech. Des. Syst. Manuf.* **5**(1), 54–69 (2011).
- [19] E. J. Lopez, D. Servin De La Mora-Pulido, R. Servin De La Mora-Pulido, F. J. Ochoa-Estrella, M. Acosta Flores and G. Luna-Sandoval, "Modeling in two configurations of a 5R 2-DoF planar parallel mechanism and solution to the inverse kinematic modeling using artificial neural network," *IEEE Access* **9**, 68583–68594 (2021).
- [20] M. D. Ratolihar and R. Prasanth Kumar, "Optimized design of 5R planar parallel mechanism aimed at gait-cycle of quadruped robots," *J. Vibroeng.* **24**(1), 104–115 (2022).
- [21] J. Shengqi, Y. Cheng, R. Luc and J. Lesley, "Five Bar Planar Manipulator Simulation and Analysis by Bond Graph," **In: Proceedings of ASME 2014 International Mechanical Engineering Congress and Exposition, IMECE2014-37116**, Montreal, Quebec (2014).
- [22] R. Roskam and R. Luc, "Five Bar Parallel Plotter based on Construction Kits and Open Source Development Environment," **In: Proceedings of 9th International Conference on Control, Mechatronics and Automation (ICCMMA)** (2021) pp. 182–187.
- [23] F. C. Can and H. Şen, "Real Time Controlled Two DOF Five Bar Robot Manipulator," **In: Proceedings of the International Symposium of Mechanism and Machine Science, AzC IFToMM** (Baku, Azerbaijan Technical University, 2017) pp. 50–56.
- [24] K. Luck and K.-H. Modler, *Getriebetechnik, Analyse - Synthese - Optimierung* (Akademie-Verlag, Berlin, 1990).
- [25] C. Gosselin and J. Angeles, "Singularity analysis of closed-loop kinematic chains," *IEEE Trans. Robot. Autom.* **6**(3), 281–290 (1990).
- [26] T. Yoshikawa, "Manipulability of robotic mechanisms," *Int. J. Robot. Res.* **4**(2), 3–9 (1985).
- [27] S. Patel and T. Sobh, "Manipulator performance measures - a comprehensive literature survey," *J. Intell. Robot. Syst.* **77**(3-4), 547–570 (2015).
- [28] A. Oarcea, A. M. F. Luputi, V. Cobilean, S.-D. Stan and E.-C. Lovasz, "Kinematic Performance Analysis of a 3-R(RPRGR)RR Planar Parallel Robot," **In: Proceedings of the 1st Workshop IFToMM for Sustainable Development Goals, I4SDG. 2021 Virtual Online, Series: Mechanisms and Machine Science**, vol. 108 (Springer, Cham, 2022) pp. 461–470.
- [29] A. M. F. Luputi, E.-C. Lovasz, M. Ceccarelli, C. Sticlaru and A.-M. Scurt (Stoian), "Kinematic study of feasibility of geared planar parallel manipulator," *Proc. Inst. Mech. Eng. Part C J. Mech. Eng. Sci.* **236**(18), 10001–10016 (2022).
- [30] J. K. Salisbury and J. J. Craig, "Articulated hands: Force control and kinematic issues," *Int. J. Robot. Res.* **1**(1), 4–17 (1982).
- [31] K.-M. Lee and R. Johnson, "Static Characteristics of an In-parallel Actuated Manipulator for Clamping and Bracing Applications," **In: Proceedings of the IEEE International Conference on Robotics and Automation** (1989) pp. 1408–1413.
- [32] H. Alt, "Der Übertragungswinkel und seine Bedeutung für das Konstruieren periodischer Getriebe," *Werkstattechnik* **26**, 61–64 (1932).
- [33] Y. Takeda and H. Funabashi, "Motion transmissibility of in-parallel actuated manipulators," *JSME Int. J. Ser. C Dyn. Control Robot. Des. Manuf.* **38**(4), 749–755 (1995).
- [34] C. Chen and J. Angeles, "Generalized transmission index and transmission quality for spatial linkages," *Mech. Mach. Theory* **42**(9), 1225–1237 (2007).
- [35] J. Wang, C. Wu and X.-J. Liu, "Performance evaluation of parallel manipulators: Motion/force transmissibility and its index," *Mech. Mach. Theory* **45**(10), 1462–1476 (2010).